eLIFE elifesciences.org

RESEARCH ARTICLE

Figures and figure supplements

Coordinated recruitment of Spir actin nucleators and myosin V motors to Rab11 vesicle membranes

Olena Pylypenko *et al*

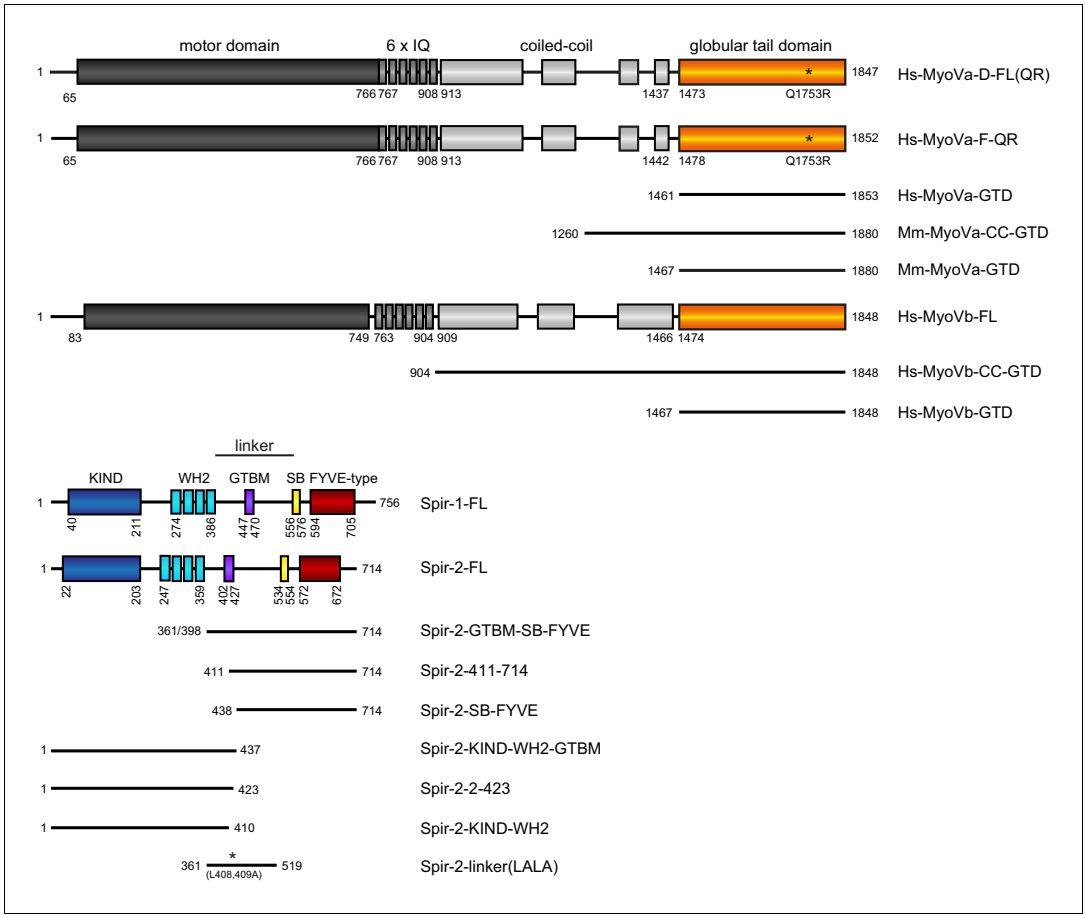

Figure 1. Schematic overview of the Spir and MyoV protein fragments used in this study. The myosin V motor domain and its 6 IQ lever arm is followed by a coiled-coil dimerization region and the C-terminal globular tail domain. The central linker region of Spir connects the N-terminal KIND and four actin binding WH2 domains on one side, with the C-terminal Spir-box (SB) and a membrane binding FYVE-type zinc finger on the other. The newly identified Spir myosin V binding motif (GTBM) is located in the middle of the linker region. The domain boundaries are indicated in the full-length MyoVa (containing exon D (D) or exon F (F)), MyoVb, Spir-1 and Spir-2 proteins. Numbers indicate amino acids. Stars indicate amino acid substitutions. *FL*, full-length; *GTD*, globular tail domain; *CC*, coiled-coil; *KIND*, kinase non-catalytic C-lobe domain; *GTBM*, globular tail domain binding motif; *SB*, Spir-box; *LALA*, L408,409A substitution. Species abbreviations are Hs, *Homo sapiens*; Mm, *Mus musculus*.
DOI: 10.7554/eLife.17523.002

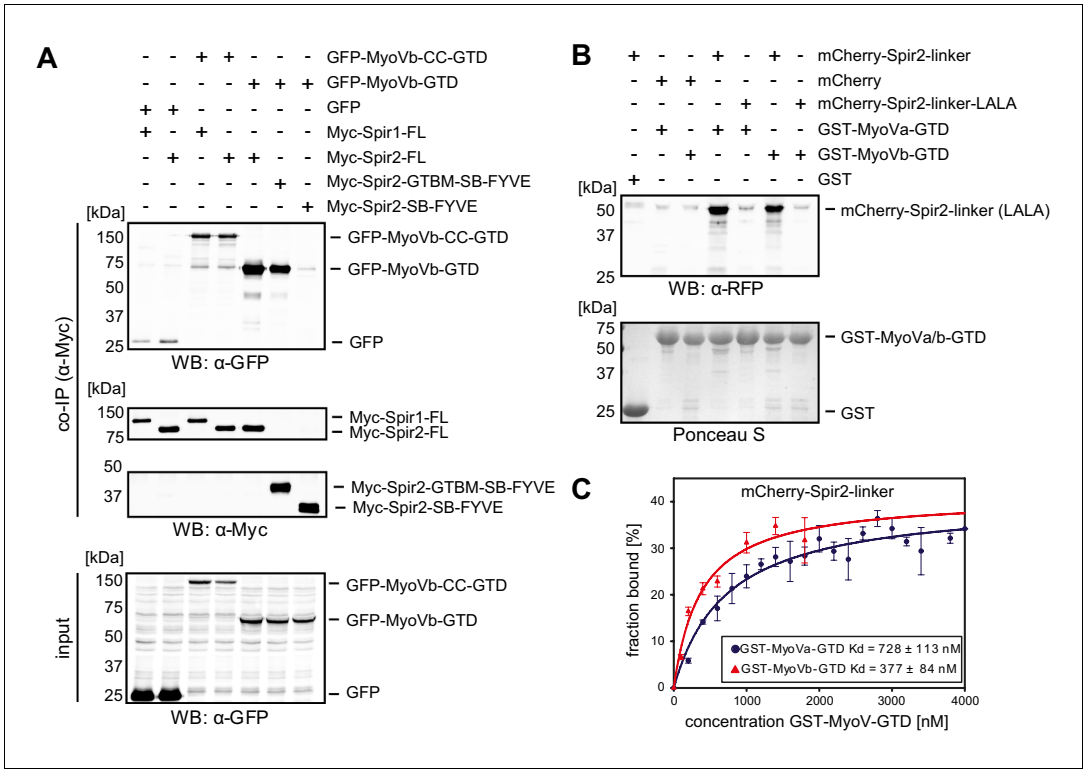

Figure 2. Spir proteins directly interact with myosin V. (**A**) Co-immunoprecipitation assay of HEK293 cells transfected with plasmids expressing AcGFP (GFP), AcGFP-tagged MyoVb deletion mutants and indicated Myc-epitope tagged Spir-1 and Spir-2 proteins. Cell lysates were immunoprecipitated with anti-Myc antibodies. The cell lysates (input) and immunoprecipitates (co-IP) were analyzed by immunoblotting with antibodies as indicated. The Spir-2-GTBM and the MyoVb globular tail domain (GTD) were identified as being essential for the Spir/MyoV interaction. N = 4 experimental repeats. *WB*, Western blotting. (**B**) GST-pulldown studies employing purified bacterially expressed recombinant proteins to analyze a direct interaction of Spir-2-linker and MyoVa/Vb-GTD. The mutation of two highly conserved leucines within the Spir-2-GTBM to alanines (human Spir-2-L408A, L409A; Spir-2-linker-LALA, see also ***Figure 4A***) largely impairs binding of this mutant to GST-MyoVa/Vb-GTD. N = 4 experimental repeats. (**C**) Fluorescence spectroscopy was used to determine the dissociation constants (K_d) for MyoVa and MyoVb GTD binding to His_6-mCherry-Spir-2-linker. *Error bars* represent SEM (n = 4 experimental repeats).

DOI: 10.7554/eLife.17523.003

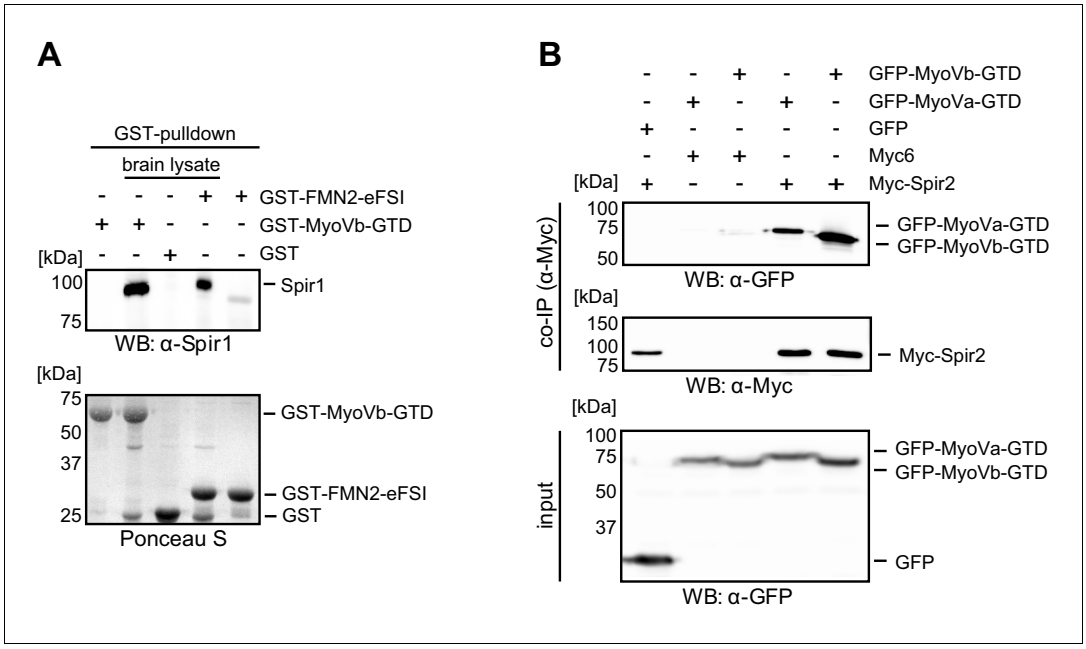

Figure 2—figure supplement 1. Interaction of endogenous Spir-1 with MyoVb-GTD. (**A**) GST-pulldown of Spir-1 proteins from mouse brain lysates. Both, GST-MyoVb-GTD and GST-FMN2-eFSI were able to pull Spir-1 from brain lysates as detected by immunoblotting (anti-Spir-1). Ponceau S staining showed equal loading of GST-fusion proteins. N = 3 experimental repeats. (**B**) The MyoVa and MyoVb globular tail domains interact with Spir-2. Co-immunoprecipitation experiments showing a co-precipitation of AcGFP-tagged MyoVa/Vb-GTD (GFP-MyoVa/Vb-GTD) with full-length Myc-epitope-tagged Spir-2 (Myc-Spir-2), which was not observed with GFP and Myc-epitope (Myc_6) controls. The proteins were transiently expressed in HEK293 cells. N = 2 experimental repeats.
DOI: 10.7554/eLife.17523.004

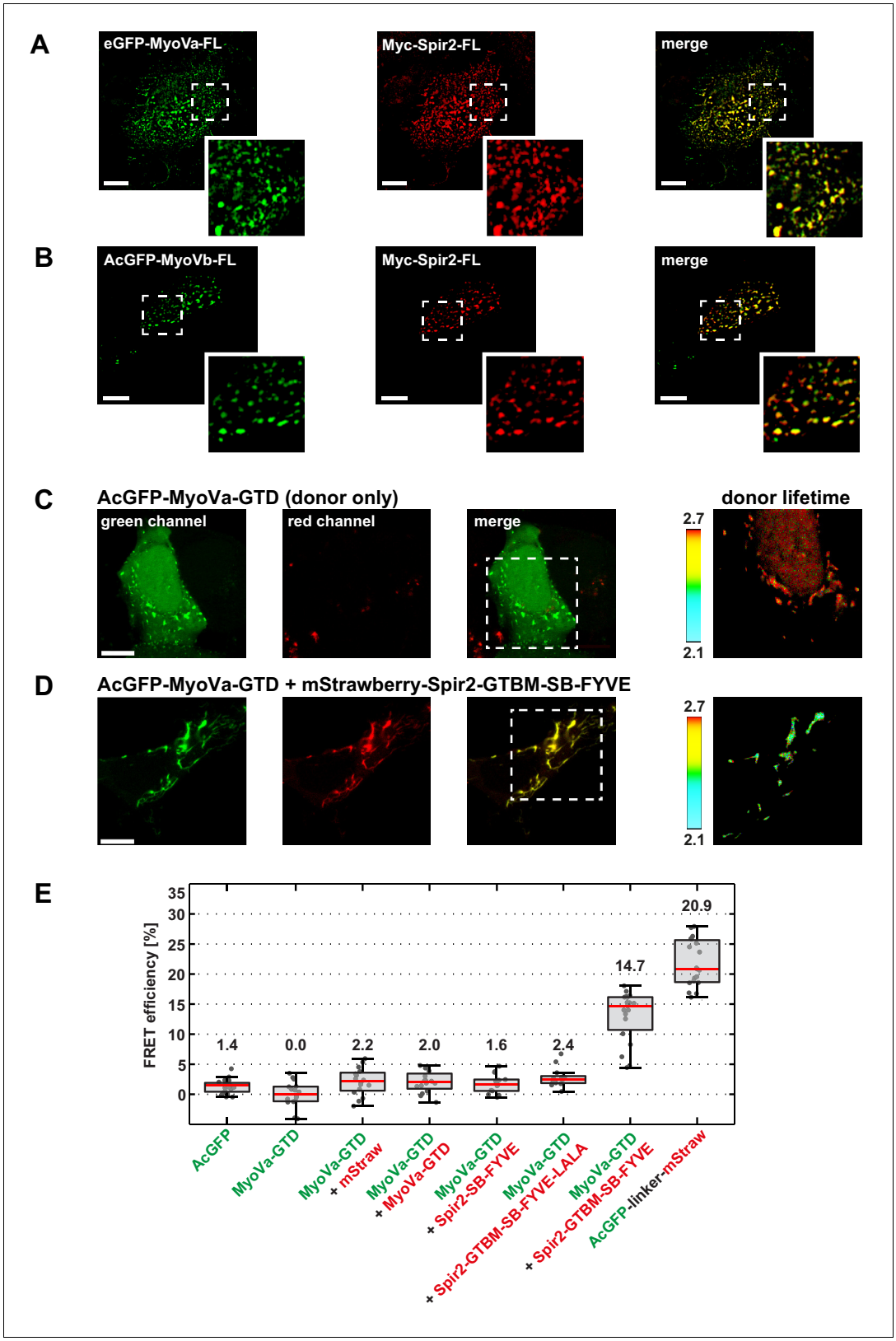

Figure 3. Myosin V and Spir-2 interact at vesicle membranes. (**A** and **B**) GFP-tagged full-length MyoVa (eGFP-MyoVa-FL; green; **A**) and MyoVb (AcGFP-MyoVb-FL; green; **B**) colocalize with Myc-epitope-tagged full-length Spir-2 (Myc-Spir-2; red) at vesicle membranes when transiently co-expressed in HeLa cells as indicated by overlapping

Figure 3 continued on next page

Figure 3 continued

punctae (merge; yellow; higher magnification in insets). 5 cells were recorded and one representative cell is presented here. *Scale bars* represent 10 μm. (**C–E**) FLIM-FRET analysis of transiently expressed AcGFP-tagged MyoVa-GTD (AcGFP-MyoVa-GTD, donor) and mStrawberry-tagged C-terminal Spir proteins (acceptors) at vesicle membranes in HeLa cells. (**C**, **D**) Examples demonstrating the lifetime shift due to FRET. Confocal fluorescence images (green channel, AcGFP; red channel, mStrawberry; and fluorescence lifetime images of AcGFP) of AcGFP-MyoVa-GTD expressed alone (**C**) and in the presence of the interacting acceptor protein mStrawberry-Spir-2-GTBM-SB-FYVE (**D**) are shown. (**E**) The average FRET efficiencies per cell measured at vesicle membranes for the indicated transiently expressed donor-acceptor combinations are presented in a box-and-whisker plot. Every dot represents a single cell. The region of interest was manually confined to the cytoplasm (average FRET efficiencies for AcGFP alone and the tandem AcGFP-linker-mStrawberry). For all other experiments, the ROI was further reduced by a threshold algorithm that identifies vesicles in the AcGFP channel. Box-and-whisker plots indicate 2nd and 3rd quartile (box), median (red horizontal line, value noted above each box), and 1.5x interquartile range (whiskers). 10–15 cells have been analyzed for each transfection.

DOI: 10.7554/eLife.17523.005

The following source data is available for figure 3:

Source data 1. Source data for FLIM-FRET analysis of MyoVa and Spir-2 expression at vesicle membranes.

DOI: 10.7554/eLife.17523.006

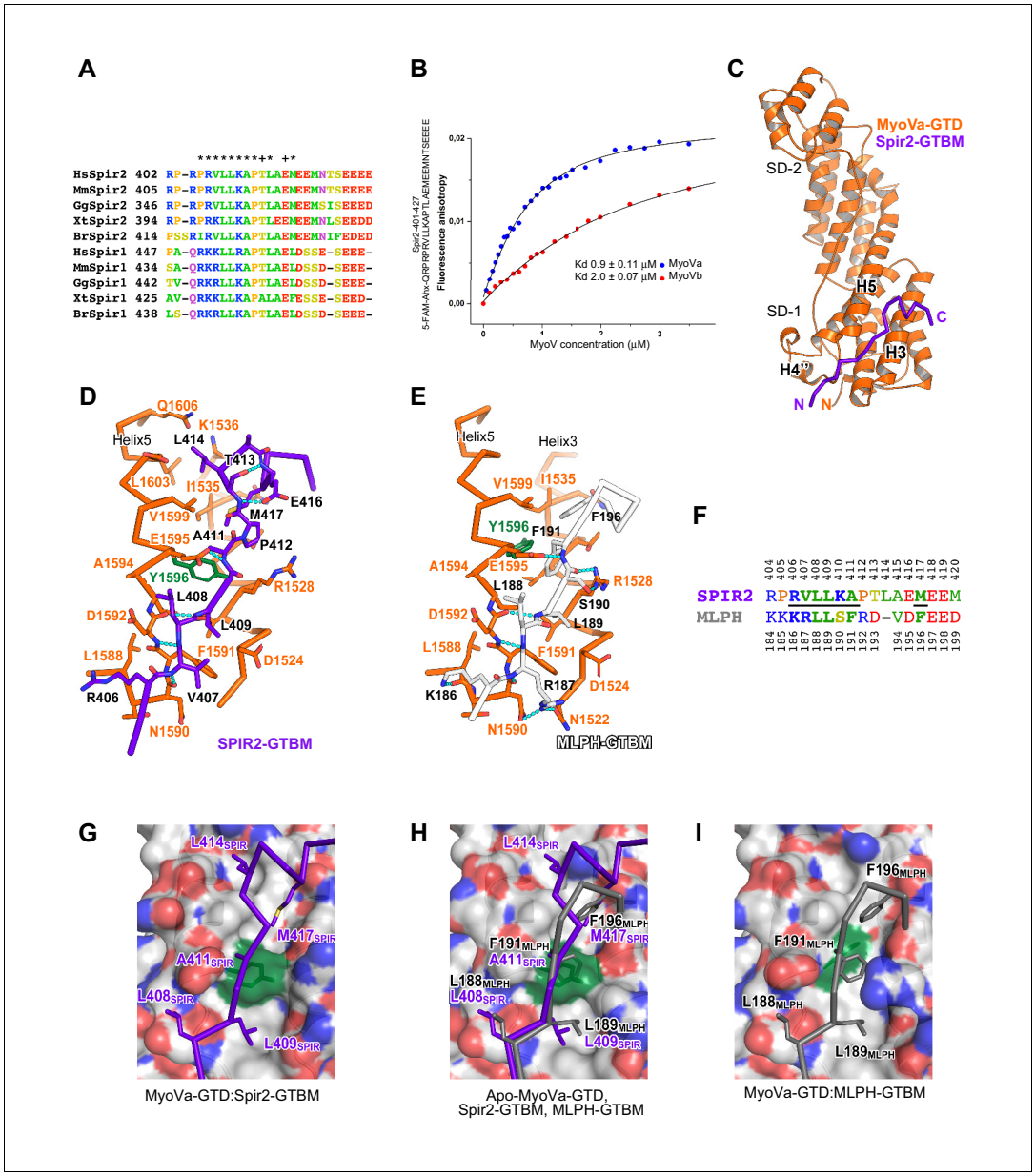

Figure 4. A conserved sequence motif of Spir binds to MyoV-GTD. (**A**) A short highly conserved sequence motif within the central Spir linker region is responsible for myosin V binding. Alignment of vertebrate Spir-1 and Spir-2 sequence fragments. The short sequence motif of about 27 amino acids in the middle part of the Spir linker region shows high sequence homology (see also ***Figure 4—figure supplement 1***). Species abbreviations: *Homo sapiens* (Hs), *Mus musculus* (Mm), *Gallus gallus* (Gg), *Xenopus tropicalis* (Xt), *Brachydanio rerio* (Br). All sequence-related data are available through CyMoBase (http://www.cymobase.org). Hs-Spir-2 residues contacting MyoVa within 4 Å distance are labeled with '*'; the Spir-2 conformation is stabilized by two conserved residues (see panel D) indicated with '+'. (**B**) Fluorescence anisotropy measurements of the binding of the Fluorescein-Spir-2-GTBM peptide (human, amino acid residues 401–427) to the MyoVa and MyoVb GTDs. The equilibrium dissociation constants (K_d) for MyoVa and MyoVb GTDs were determined by fitting the titration curves as detailed in the Materials and Methods section. The experiments were repeated twice with two different protein preparations. (**C**) Crystal structure of the MyoVa-GTD:Spir-2-GTBM complex. Spir-2-GTBM (purple) binds to subdomain-1 (SD-1) of MyoVa-GTD (orange). (**D**) Close-up view of the Spir-2-GTBM bound to MyoVa-GTD. Residues forming the interaction sites are shown as sticks and are labeled. Spir-2 E416 and T413 form intramolecular hydrogen bonds (dashed lines). Spir-2 V407, L409 and MyoVa N1590 and D1592 backbone atoms form an intermolecular β-structure like hydrogen bond network. (**E**) MLPH-GTBM bound to MyoVa-GTD (PDB ID 4LX2). The N-terminal part of MLPH-GTBM (residues from K186 to L189) interacts with MyoVa in a similar manner to Spir-2 (residues 406–409). A similar

Figure 4 continued on next page

Figure 4 continued

hydrogen bond between MyoVa E1595 and the main chain nitrogen of MLPH F191 is also observed in the Spir-2:MyoVa interface. (**F**) Structure based sequence alignment of the Spir-2-GTBM and MLPH-GTBM fragments. Residues making similar contacts with MyoVa are highlighted with a black line. (**G**) Hydrophobic residues anchoring Spir-2-GTBM on the MyoVa-GTD surface. Spir-2 A411 is packed on the top of MyoVa Y1596 (green) side chain (see also panel D). (**H**) Spir-2 (purple) and MLPH (gray) GTBMs docked on the surface of apo-MyoVa-GTD (PDB ID 4LX1). The apo-MyoVa-GTD hydrophobic cleft between the H5 and H3 is compatible with Spir-2 binding, but not with MLPH, where the side chain of F191 clashes with MyoVa Y1596 (green). In Spir, the conserved L414 side chain anchors the C-terminal Spir-2 fragment extending the interacting hydrophobic surface compared to what is found for MLPH-GTBM binding. (**I**) Hydrophobic residues anchoring MLPH-GTBM in the MyoVa-GTD pocket (PDB ID 4LX2). The MyoVa Y1596 (green) side chain is rotated to bury the side chain within the protein core (see also panel E) to accommodate MLPH F191 in the binding pocket.

DOI: 10.7554/eLife.17523.007

Figure 4—figure supplement 1. Gene and protein sequence structures of vertebrate Spir. (**A**) Exon/intron structure of human Spir-1 and Spir-2. The location of the fourth WH2 domain, MyoV binding motif (GTBM), Spir-box (SB) and FYVE-type zinc-finger is indicated. (**B**) Alignment of vertebrate Spir-1 and Spir-2 sequences starting from the last WH2 domain to the FYVE-type zinc finger. High sequence homology between all sequences was only observed for the WH2 domain, the Spir-box, the FYVE-type zinc finger and the GTBM, but not for the rest of the linker region. Species abbreviations are: *Homo sapiens* (Hs), *Mus musculus* (Mm), *Gallus gallus* (Gg), *Xenopus tropicalis* (Xt), *Brachydanio rerio* (Br). All sequence_related data are available through CyMoBase (http://www.cymobase.org).

DOI: 10.7554/eLife.17523.008

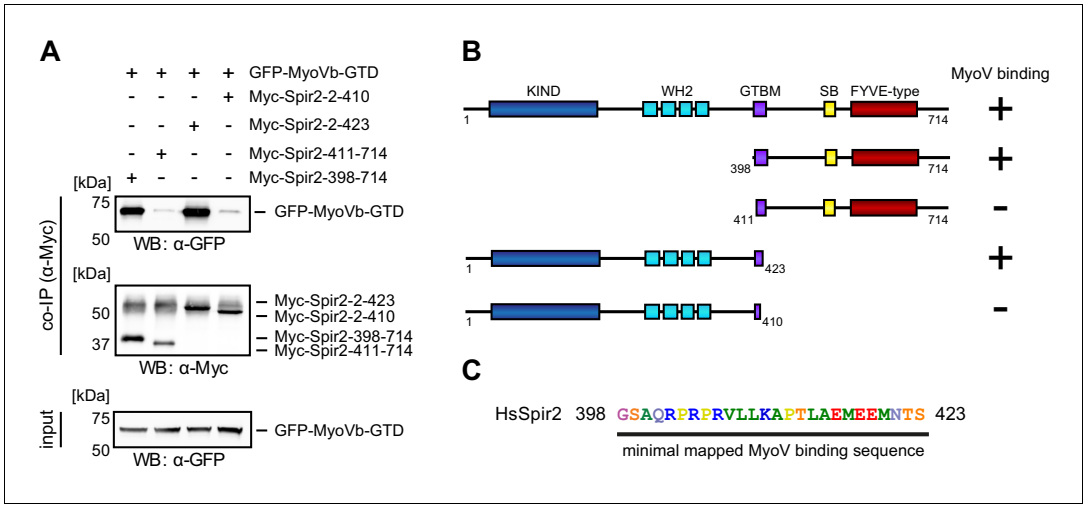

Figure 4—figure supplement 2. Mapping of the Spir-2 myosin binding domain. (**A**) Co-immunoprecipitation experiments employing AcGFP-tagged MyoVb-GTD (GFP-MyoVb-GTD) as well as N-terminal and C-terminal Spir-2 deletion mutants show myosin V co-precipitation with the C-terminal Myc-Spir-2-398-714 protein and the N-terminal Myc-Spir-2-2-423 protein, but not with C-terminal Myc-Spir-2-411-714 protein and the N-terminal Myc-Spir-2-2-410 protein. Numbers indicate amino acids. N = 2–4 experimental repeats. (**B**) Overview of the Spir-2 deletion mutants used in (**A**) compared to full-length Spir-2 and their capacity to bind (+) or not bind (–) to MyoVb-GTD. (**C**) The minimal mapped Spir-MyoV interaction sequence of human Spir-2 contains amino acids 398 to 423.

DOI: 10.7554/eLife.17523.009

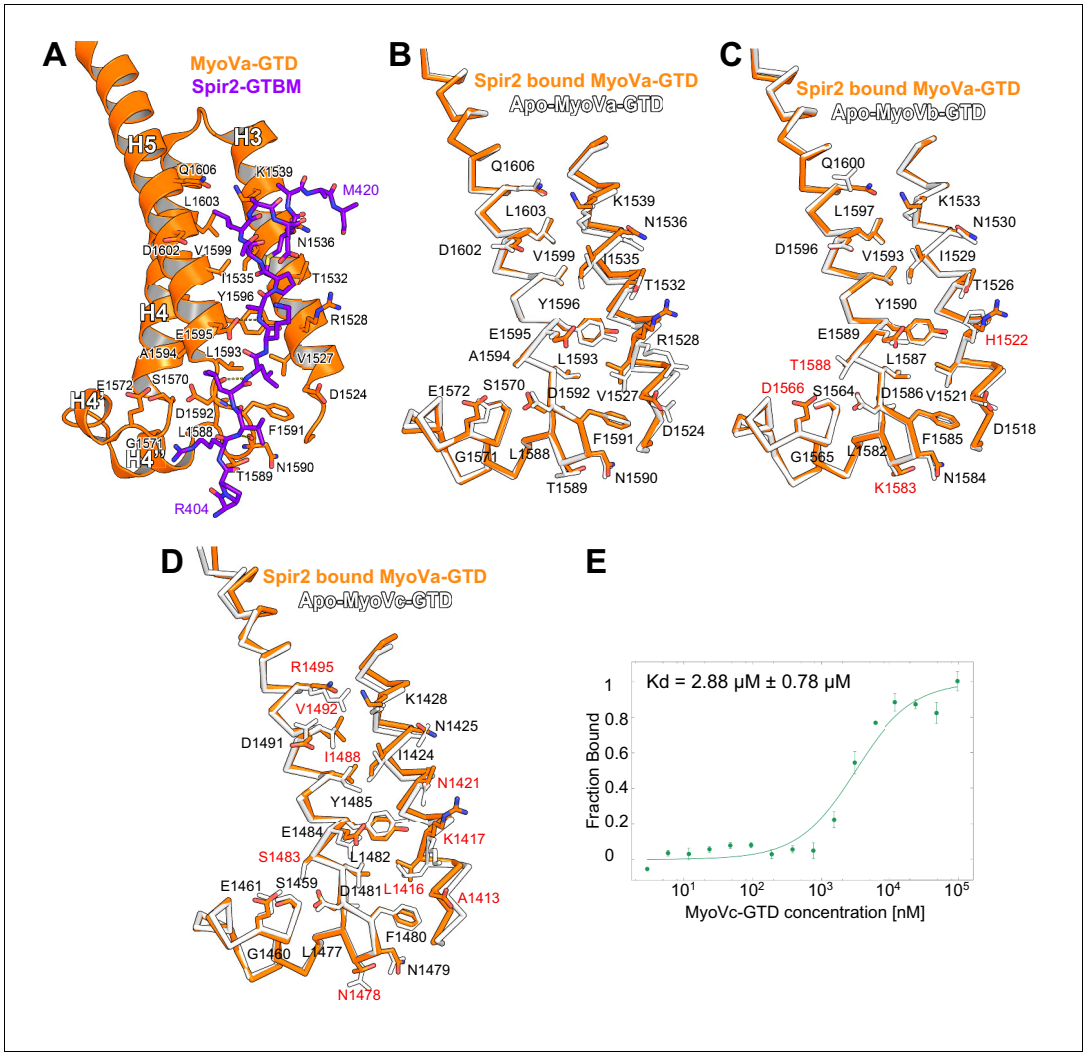

Figure 4—figure supplement 3. Comparison of myosin V isoforms Spir/MLPH binding sites. (**A**) Spir-2-GTBM (purple), represented in sticks, bound to MyoVa-GTD (orange). Shown in orange sticks and labeled are the side chains of the MyoVa-GTD residues whose solvent accessible area is reduced upon complex formation. Hydrogen bonds are represented as dashed lines. (**B**) MyoVa-GTD undergoes minor conformational change upon Spir-2-GTBM binding. MyoVa bound to Spir-2-GTBM is shown in orange while apo-MyoVa (PDB ID 4LX1) is white. Upon Spir-2 binding MyoVa, H3 is shifted along the helix axis by 0.9Å and the side chains of Y1596, F1591, K1539, R1528 change slightly their orientations to accommodate the partner. (**C**) The MyoVb structure is compatible with Spir-GTBM binding. The Spir-2-GTBM binding site is almost identical in MyoVa-GTD (orange) and MyoVb-GTD (PDB ID 4J5M) (white) (***Nascimento et al., 2013***). Residue labeling corresponds to the MyoVb sequence. Residues that are not identical in the MyoVb and MyoVa sequences are labeled in red. (**D**) MyoVc binds Spir-GTBM. The Spir-2-GTBM binding site is similar in MyoVa-GTD (orange) and MyoVc-GTD (PDB ID 4L8T) (white) (***Nascimento et al., 2013***). Residue labeling corresponds to the MyoVc sequence, the labels for identical residues are in black and for homologous residues in red. (**E**) Fluorescin-Spir-2-GTBM peptide (human, amino acids 401–427) binding to MyoVc-GTD measured by microscale thermophoresis. N = 3 experimental repeats.

DOI: 10.7554/eLife.17523.010

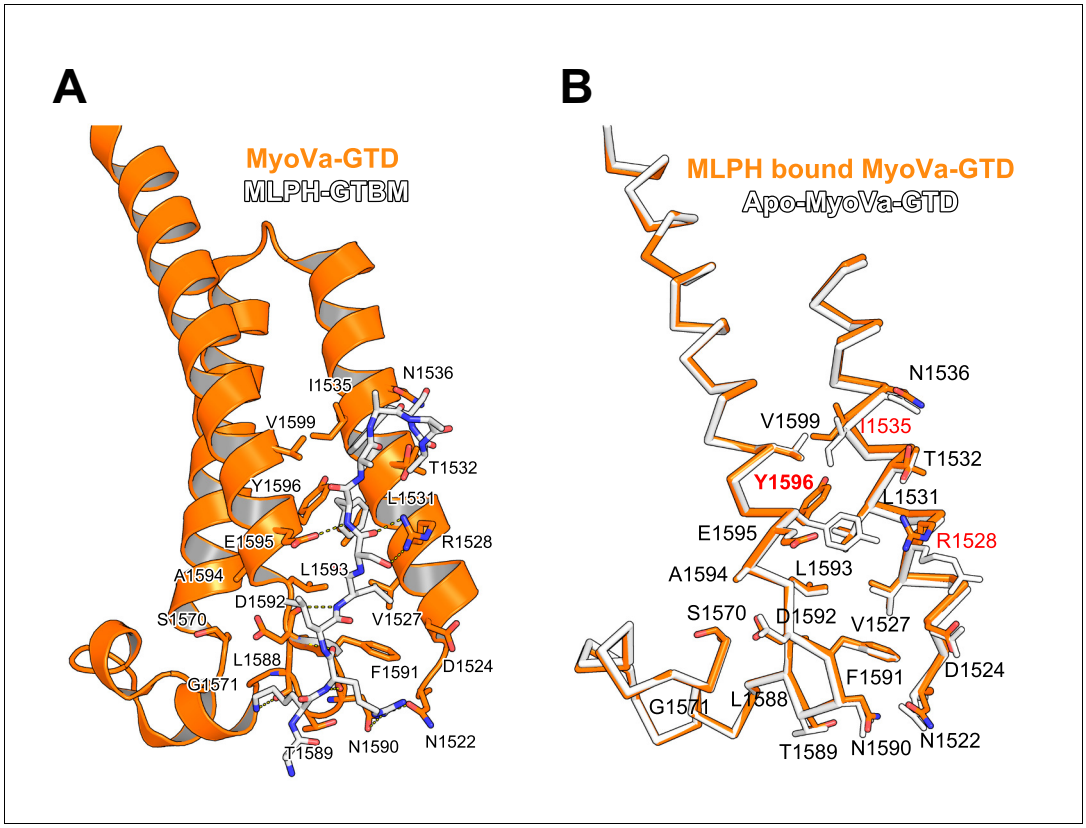

Figure 4—figure supplement 4. MyoVa conformational change upon MLPH binding. (**A**) MLPH-GTBM (white), represented in sticks, bound to MyoVa-GTD (orange). Shown in orange sticks and labeled are the side chains of MyoVa-GTD residues whose solvent accessible area is reduced upon complex formation. Hydrogen bonds are represented as dashed lines. (**B**) MyoVa-GTD conformational change upon MLPH-GTBM binding. MLPH-GTBM bound MyoVa is orange, apo-MyoVa-GTD (PDB ID 4LX1) is white. MLPH-GTBM binding requires a small (0.5 Å) shift of MyoVa H3 along the helix axis; and conformational changes of Y1596, I1535 and R1528 side chains.
DOI: 10.7554/eLife.17523.011

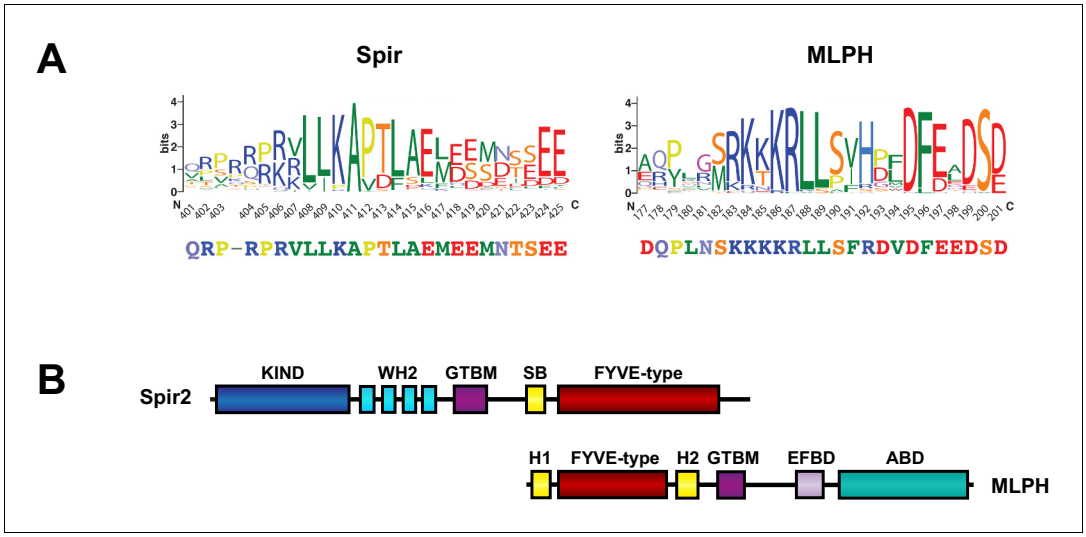

Figure 4—figure supplement 5. Structural similarities of Spir and melanophilin. (**A**) Spir-GTBM sequence logo indicates the sequence conservation in Spir-1 and Spir-2 proteins; MLPH-GTBM sequence logo demonstrates the sequence conservation in MLPH proteins. WebLogos (***Crooks et al., 2004***) were generated from respective parts of the alignment of 223 Spir sequences and 44 MLPH sequences after reducing redundancy with CDhit (***Li and Godzik, 2006***) applying a 90% sequence similarity cut-off. The Spir and MLPH motifs involved in binding the MyoV globular tail domain have a similar charge distribution (the N-terminal sequence is positively charged and the C-terminal sequence is negatively charged). Both fragments have two conserved leucine residues in the N-terminal part of the binding motif. (**B**) Comparison of the Spir-2 and MLPH domain composition. Both MyoV interacting proteins share a GTBM which is linked to a putative small GTPase interacting Spir-Box (SB) in Spir-2 or synaptotagmin-like protein homology domains (H1 and H2) in MLPH and FYVE-type membrane binding units. The MLPH N-terminal region encompassing the H1 FYVE-type H2 region interacts with the Rab27 GTPase (***Kukimoto-Niino et al., 2008***). Despite its structural similarity to membrane binding domains, a direct interaction of the MLPH FYVE-type domain has not yet been addressed. MLPH also contains a second MyoVa exon-F binding domain (EFBD), and an F-actin binding domain (ABD) at the C-terminus.

DOI: 10.7554/eLife.17523.012

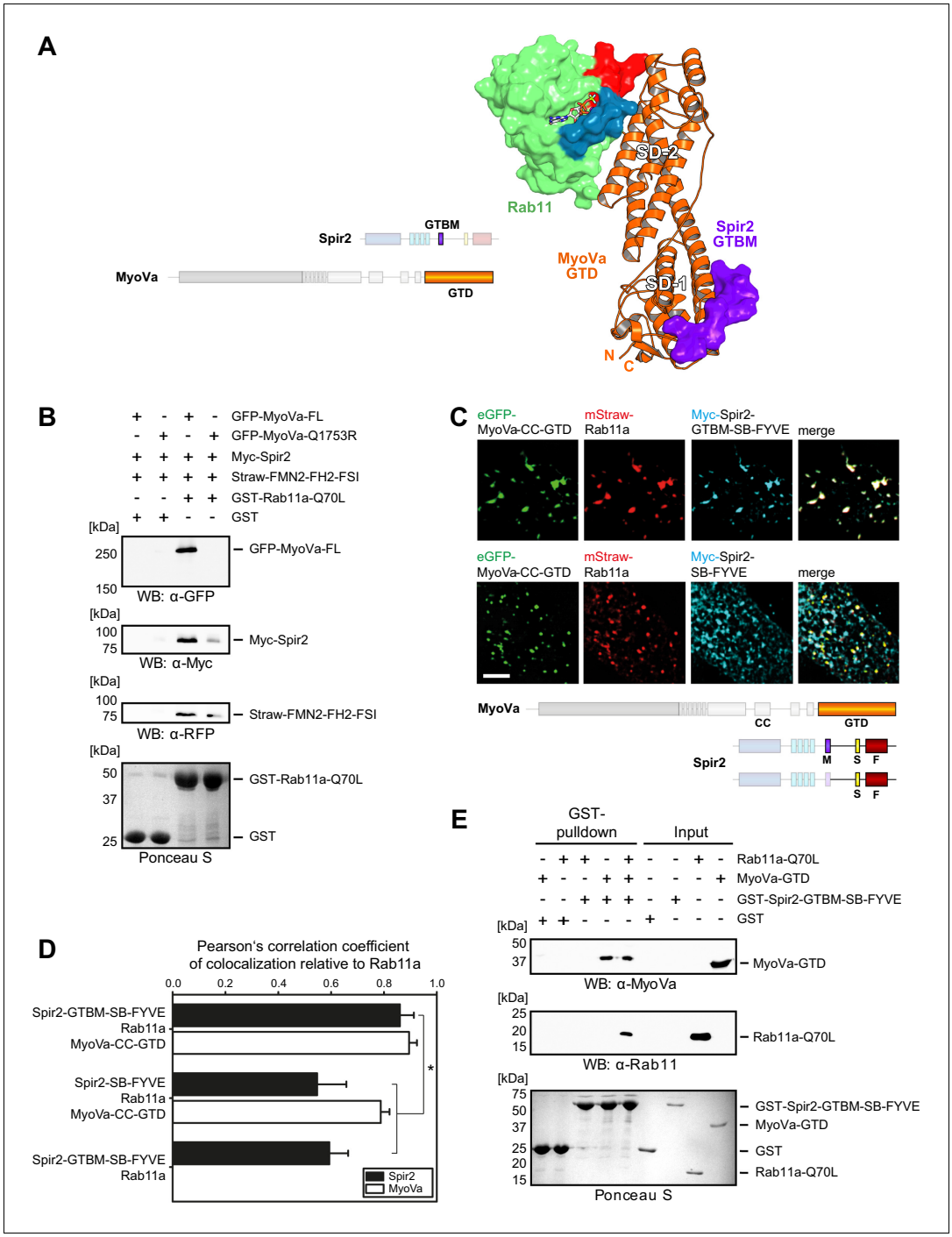

Figure 5. Myosin V links Spir-2 and Rab11 into a tripartite complex. (**A**) A model of the Rab11a:MyoVa-GTD:Spir-2-GTBM complex was generated by superimposition of the MyoVa-GTD from the two crystal structures Rab11a:MyoVa-GTD and MyoVa-GTD:Spir-2-GTBM. The Spir-2-GTBM (purple) binds to the SD-1 of the MyoVa-GTD (orange) and Rab11a (green, Switch-1 blue, Switch-2 red) binds to its SD-2. (**B**) GST-pulldown assay with purified GTP-locked GST-Rab11a-Q70L mutant and HEK293 cell lysates transiently over-expressing full-length Myc-epitope-tagged Spir-2 (Myc-Spir-2), mStrawberry-tagged C-terminal formin-2 (Straw-FMN2-FH2-FSI), eGFP-tagged full-length MyoVa (GFP-MyoVa-FL) or eGFP-tagged full-length MyoVa with the Q1753R mutation, which disrupts interaction with Rab11, (GFP-MyoVa-Q1753R). GST-Rab11a-Q70L is able to pull GFP-MyoVa-FL from cell lysates, but not the GFP-MyoVa-Q1753R mutant. In the presence of GFP-MyoVa-FL, GST-Rab11a-Q70L is also able to pull down Myc-Spir-2, as well as Straw-FMN2-FH2-FSI. Only faint Myc-Spir-2 and Straw-FMN2-FH2-FSI bands were detected with the GFP-MyoVa-Q1753R mutant. N = 2 experimental repeats. (**C**) The localization of transiently co-

Figure 5 continued on next page

Figure 5 continued

expressed tagged Rab11 (mStrawberry, mStraw-Rab11; red), MyoVa-CC-GTD (eGFP, eGFP-MyoVa-CC-GTD; green) and the Myc-epitope tagged (Myc, cyan) C-terminal Spir-2 proteins encoding (Myc-Spir-2-GTBM-SB-FYVE) or lacking (Myc-Spir-2-SB-FYVE) the MyoV binding motif was analyzed by fluorescence microscopy. Deconvoluted pictures indicate the localization of the proteins on vesicular structures. *Scale bars* represent 5 μm. 5 cells were recorded for each condition and the cytoplasmic region of one representative cell is presented here. (**D**) The colocalization of tagged proteins as described in (**C**) was quantified for the indicated co-expressions by determining its Pearson's correlation coefficient (PCC) as shown in a bar diagram. Each bar represents the mean PCC value for at least 4 cells analyzed. *Error bars* represent SEM. Statistical analysis was done using Student's t-test to compare two co-expression conditions with a confidence interval of 95%. *p<0.05. ***Figure 5D***. (**E**) GST-pulldown assay engaging purified GST-tagged Spir-2-GTBM-SB-FYVE protein, purified MyoVa-GTD and the purified GTP-locked Rab11a-Q70L mutant. GST-Spir-2-GTBM-SB-FYVE alone does not interact with Rab11a-Q70L. In contrast, the presence of the MyoVa-GTD allows GST-Spir-2-GTBM-SB-FYVE to pull Rab11a-Q70L, as indicated by immunoblotting with antibodies recognizing MyoVa and Rab11a. N = 3 experimental repeats.

DOI: 10.7554/eLife.17523.014

The following source data is available for figure 5:

Source data 1. Source data for calculation of mean PCC values for colocalization analysis.

DOI: 10.7554/eLife.17523.015

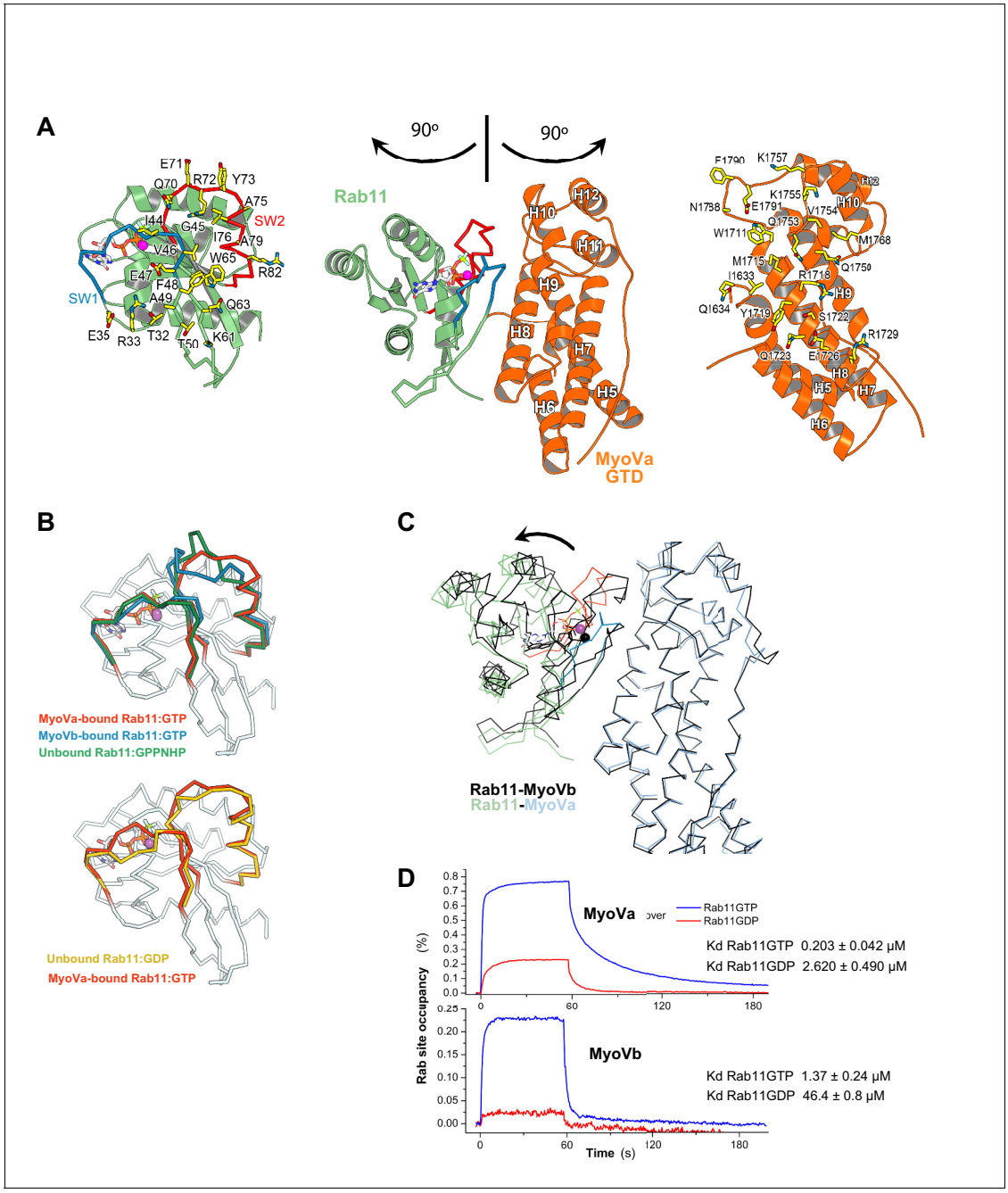

Figure 5—figure supplement 1. Rab11 binds to MyoVa-GTD at the same site as to MyoVb-GTD, but adopts a different conformation in the two complexes. (**A**) Structure of Rab11-GTP bound to the MyoVa-GTD SD-2 (SD-1 is not shown for simplicity), the nucleotide is shown in sticks. The MyoVa interaction epitope of Rab11 (left) and the Rab11 binding site of MyoVa (right) are shown in sticks and labeled. Rab11 switch 1 and switch 2 are shown in blue and red. (**B**) Conformational differences in the switches of different active (top) Rab11-GTP and inactive (low) Rab11-GDP. The switch 2 conformation changes in MyoVa-bound Rab11 (red) compared to unbound Rab11:GPPNHP (PDB ID 1YZK) (green) or compared to Rab11 when bound to MyoVb (PDB ID 4LX0) (blue). Note that Rab11-GTP switch 1 also differs when it is bound to MyoVa or to MyoVb, while it is similar in the apo and MyoVa bound complex. The Rab11-GTP switch 2 conformation is similar to that of Rab11-GDP (PDB ID1OIV) (yellow) when bound to MyoVa. This is consistent with the relatively high affinity of Rab11-GDP for MyoVa (panel D). (**C**) Rab11-GTP binds with different orientations to the MyoVa and MyoVb surfaces. Rab11-MyoVb complex (black) is superimposed on Rab11-MyoVa (colored), using the SD-2 of the MyoV GTD. The shift of the Rab11 molecule is shown with an arrow. (**D**) Representative SPR binding curves recorded for Rab11-GDP and Rab11-GTP at 450 nM MyoVa-GTD and MyoVb-GTD concentrations. N = 3 experimental repeats.

DOI: 10.7554/eLife.17523.016

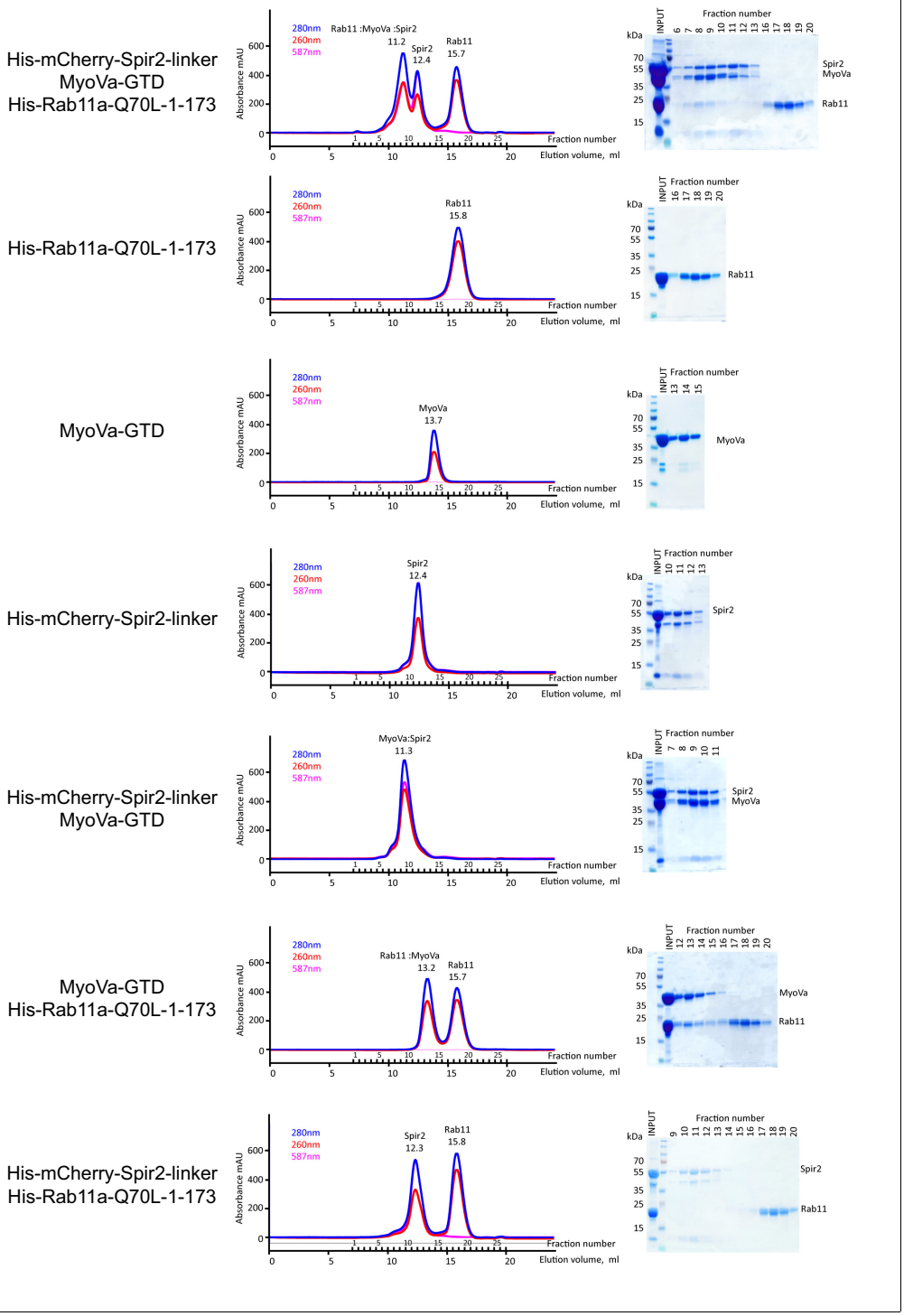

Figure 5—figure supplement 2. The MyoVa-GTD links Rab11 and Spir-2-linker into a tripartite complex. Analytical gel-filtration experiments of His_6-mCherry-Spir-2-linker: MyoVa-GTD: His_6-Rab11a-Q70L-1-173 demonstrate co-elution of the three proteins in the first peak. Individual proteins His_6-Rab11a-Q70L-1-173, MyoVa-GTD, His_6-mCherry-Spir-2-linker; two component protein complexes MyoVa-GTD:Spir-2, MyoVa-GTD:Rab11a were also analyzed. The mix of Spir-2 and Rab11 proteins eluted as individual protein components. Gel-filtration elution

Figure 5—figure supplement 2 continued on next page

Figure 5—figure supplement 2 continued

profiles (left) monitored by light absorbance at 280 nm, 260 nm and 587 nm; and SDS-PAGE analysis (right) of the eluted fractions.

DOI: 10.7554/eLife.17523.017

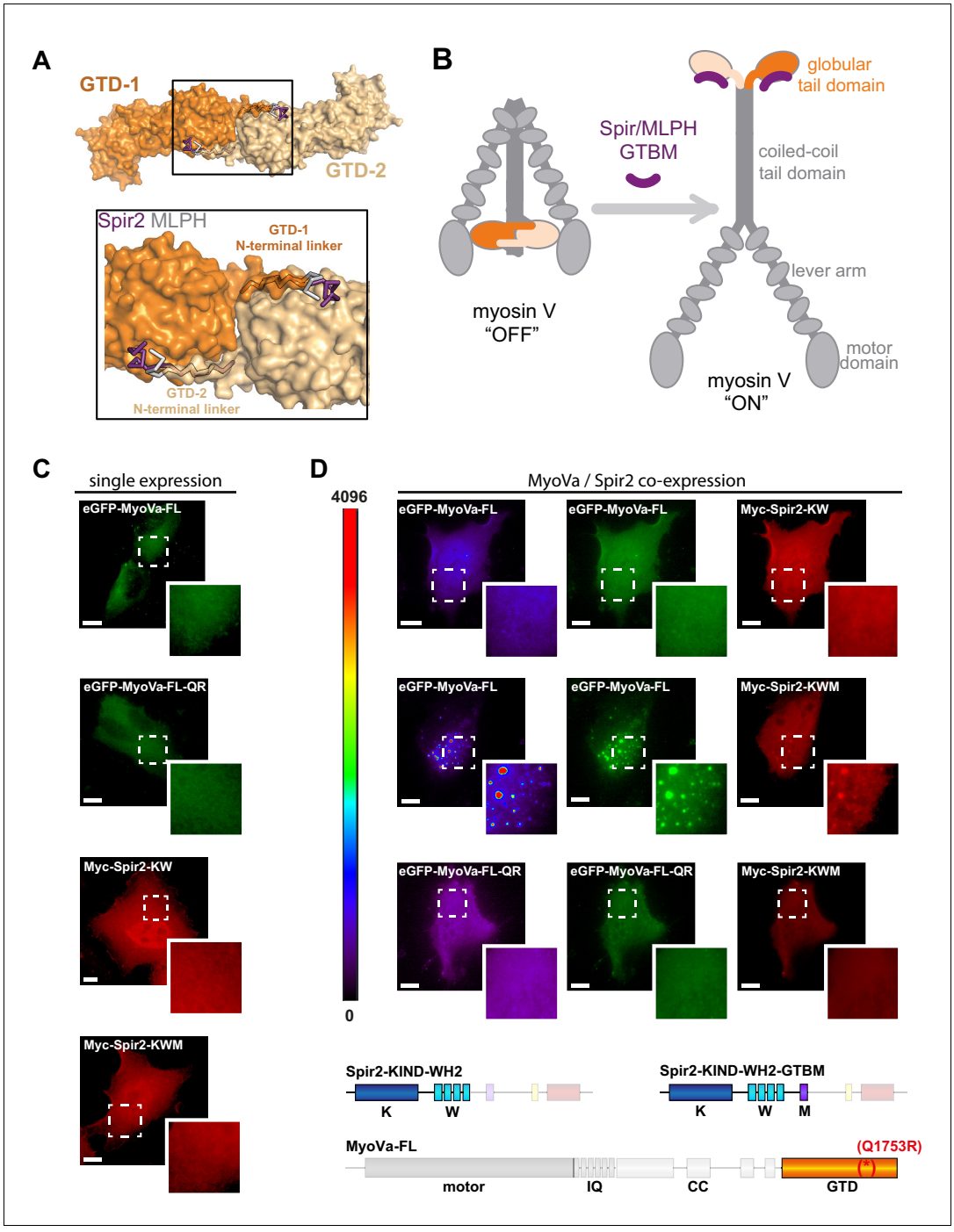

Figure 6. Spir-2 facilitates myosin V recruitment to vesicle membranes. (**A**) A putative interaction mode of the GTDs within the MyoV off state was derived from the MyoVb-GTD structure (PDB ID 4LX0). Two GTDs interact with each other via N-terminal linkers occupying the Spir/MLPH binding pockets on the neighboring GTD, Spir and MLPH GTBMs are shown in ribbon. (**B**) Schematic representation of myosin V activation by GTBM binding. (**C** and **D**) N-terminal Spir fragments target MyoVa to vesicle membranes. (**C**) N-terminal Spir fragments (Myc-Spir-2-KIND-WH2, Myc-Spir-2-KW; Myc-Spir-2-KIND-WH2-GTBM, Myc-Spir-2-KWM) and full-length MyoVa motor proteins (eGFP-MyoVa-FL, eGFP-MyoVa-FL-Q1753R) have an even cytoplasmic and nuclear localization when transiently expressed in HeLa cells (single expression). At least 5 cells were recorded for each condition and one representative cell is presented here. *Scale bars* represent 10 μm. (**D**) Expression of full-length GFP-tagged MyoVa (eGFP-MyoVa-FL; green (middle) and as heat map (left)) shows an even cytoplasmic distribution that is not changed by co-expression of the Spir-2 fragment (Myc-Spir-2-KIND-WH2), which is not able to bind to MyoV and

Figure 6 continued on next page

Figure 6 continued

lipid membranes (upper panel). In contrast, co-expression of a myosin V binding Spir-2 fragment (Myc-Spir-2-KIND-WH2-GTBM; red, middle panel) leads to targeting of MyoVa to vesicle membranes and to overlapping Spir-2 and MyoVa localization (higher magnification insets). Heat maps represent grey values for MyoVa fluorescence intensities rising from '0' (black) to '4096' (red) to document equal expression levels of MyoVa proteins in the depicted cells. To address Rab11 dependence on motor protein targeting, the GFP-tagged melanocyte specific F isoform of the Q1753R mutant MyoVa (eGFP-MyoVa-QR) that does not bind Rab11 was expressed. The expressed MyoVa mutant has an even cytoplasmic distribution that was not changed upon co-expression of the myosin V binding Spir-2 fragment (Myc-Spir-2-KIND-WH2-GTBM; red, lower panel). Representative cells are shown. All cells observed under single and co-expression conditions had a vesicular or cytoplasmic localization as shown by the representative cells presented here. 5 cells were recorded for each condition and one representative cell is presented here. *Scale bars* represent 10 μm.

DOI: 10.7554/eLife.17523.018

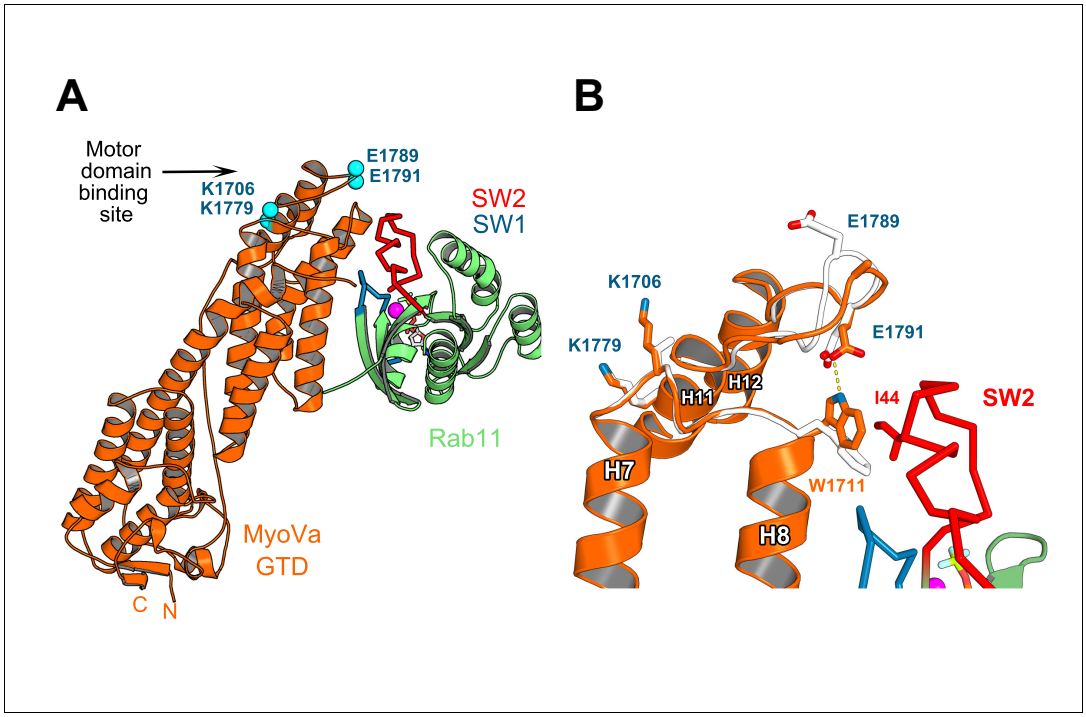

Figure 6—figure supplement 1. Rab11 binding may affect the GTD:motor-domain interaction in the folded inhibited state of MyoV. (**A**) Motor domain and Rab11 binding sites are located on the opposite sides of MyoV-GTD SD-2. Conserved MyoVa-GTD residues participating in motor domain binding in the inhibited folded conformation of MyoVa (***Yao et al., 2015***) are shown as spheres and labeled in blue. E1789 and E1791 belongs to a loop connecting MyoV H11 and H12. (**B**) Comparison of apo-MyoVa and Rab11 bound MyoVa H11-H12 loop. Close-up view of the Rab11 bound H11-H12 MyoV loop region (orange) superimposed on the apo-MyoVa structure (white). The H11-H12 loop also participates in Rab11 binding and adopts a different conformation in the Rab11:MyoVa complex. When it is not engaged in interactions, this MyoV-GTD loop might swap between different conformations. In the MyoVa:Rab11 complex, MyoVa E1791 makes a hydrogen bond (dashed line) with the conserved W1711 side chain stabilizing the residue in the conformation compatible with Rab11 binding. Thus, Rab11 binding to the folded MyoV full-length motor may retract the H11-H12 loop from the motor domain-binding interface and destabilize the full length GTD-motor domain intramolecular interactions, favoring activation of the motor.

DOI: 10.7554/eLife.17523.019

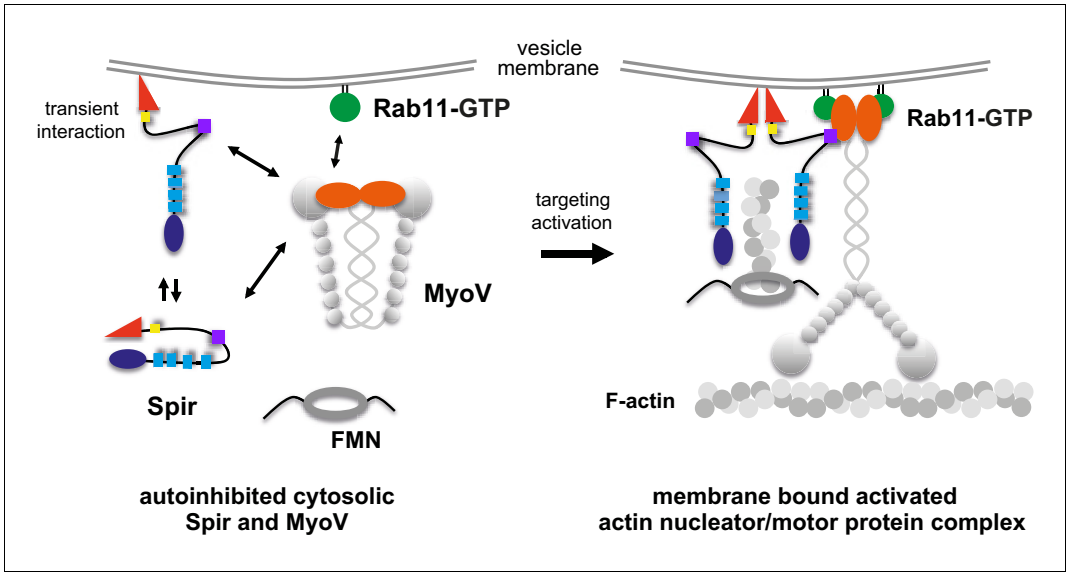

Figure 7. A model of a coordinated assembly of the Spir/FMN F-actin nucleator complex and myosin V motor proteins at Rab11 vesicle membranes. Spir and MyoV proteins adopt a backfolded autoinhibited conformation in the cytoplasm (***Li et al., 2008***; ***Liu et al., 2006***; ***Thirumurugan et al., 2006***; ***Tittel et al., 2015***). A non-specific transient interaction of the Spir FYVE-type domain with membranes opens up Spir (***Tittel et al., 2015***). Spir-GTBM binding to the inhibited MyoV contributes to the release of MyoV autoinhibition and facilitates MyoV-GTD interaction with Rab11 at vesicle membranes, further stabilizing the MyoV activated extended conformation. The Spir-FYVE membrane interaction releases the cis-regulatory KIND/FYVE domain interaction and subsequently allows formin (FMN) dimer recruitment at the membranes (***Tittel et al., 2015***). Interaction with the formin dimer promotes Spir dimerization and allows efficient F-actin nucleation (***Dietrich et al., 2013***; ***Namgoong et al., 2011***; ***Quinlan et al., 2007***). Note that the order of events is not known and will require further studies. The domain structures of the Spir and MyoV proteins are indicated by the same color code as in ***Figure 1*** (Spir: FYVE, red; Spir-box, yellow; GTBM, purple; WH2, light blue; KIND, dark blue; MyoV: GTD, orange; coiled coil, calmodulin bound IQ motifs and motor domain, gray).

DOI: 10.7554/eLife.17523.020